



**HAL**  
open science

## **First subcellular localization of the amnesic shellfish toxin, domoic acid, in bivalve tissues: Deciphering the physiological mechanisms involved in its long-retention in the king scallop *Pecten maximus***

José Luis García-Corona, Hélène Hégaret, Margot Deléglise, Adeline Marzari, Carmen Rodríguez-Jaramillo, Valentin Foulon, Caroline Fabioux

### ► To cite this version:

José Luis García-Corona, Hélène Hégaret, Margot Deléglise, Adeline Marzari, Carmen Rodríguez-Jaramillo, et al.. First subcellular localization of the amnesic shellfish toxin, domoic acid, in bivalve tissues: Deciphering the physiological mechanisms involved in its long-retention in the king scallop *Pecten maximus*. *Harmful Algae*, 2022, 116, pp.102251. 10.1016/j.hal.2022.102251 . hal-03814644

**HAL Id: hal-03814644**

**<https://hal.univ-brest.fr/hal-03814644>**

Submitted on 14 Nov 2022

**HAL** is a multi-disciplinary open access archive for the deposit and dissemination of scientific research documents, whether they are published or not. The documents may come from teaching and research institutions in France or abroad, or from public or private research centers.

L'archive ouverte pluridisciplinaire **HAL**, est destinée au dépôt et à la diffusion de documents scientifiques de niveau recherche, publiés ou non, émanant des établissements d'enseignement et de recherche français ou étrangers, des laboratoires publics ou privés.

1 **First subcellular localization of the amnesic shellfish toxin, domoic acid, in bivalve**  
2 **tissues: deciphering the physiological mechanisms involved in its long-retention in the**  
3 **king scallop *Pecten maximus***

4

5 José Luis García-Corona<sup>1</sup>, H  l  ne Hegaret<sup>1</sup>, Margot Del  glise<sup>1</sup>, Adeline Marzari<sup>1</sup>, Carmen  
6 Rodr  guez-Jaramillo<sup>2</sup>, Valentin Foulon<sup>3</sup> & Caroline Fabioux<sup>1\*</sup>

7

8 <sup>1</sup>Institut Universitaire Europ  en de la Mer, Laboratoire des Sciences de l'Environnement  
9 Marin (UMR6539 CNRS/UBO/IFREMER/IRD) Technop  le Brest-Iroise 29280, Plouzan  ,  
10 France.

11 <sup>2</sup>Centro de Investigaciones Biol  gicas del Noroeste (CIBNOR), Mar Bermejo 195, Col. Playa  
12 Palo de Santa Rita, La Paz, B.C.S. 23090, Mexico.

13 <sup>3</sup>Universit   Bretagne Loire, ENIB, UMR CNRS 6285 LabSTICC, 29238, Brest, France.

14

15 \*Corresponding author: Caroline Fabioux

16

17 Institut Universitaire Europ  en de la Mer, Laboratoire des Sciences de l'Environnement Marin  
18 (UMR6539 CNRS/UBO/IFREMER/IRD) Technop  le Brest-Iroise 29280, Plouzan  , France.

19

20 e-mail: [cfabioux@univ-brest.fr](mailto:cfabioux@univ-brest.fr)

21 **Abstract**

22 Domoic acid (DA), the phycotoxin responsible for amnesic shellfish poisoning (ASP), is an  
23 excitatory amino acid naturally produced by at least twenty-eight species of the bloom-  
24 forming marine diatoms *Pseudo-nitzschia* spp. Suspension feeders, such as bivalve mollusks,  
25 can accumulate and lengthy retain high amounts of DA in their tissues, threatening human  
26 health and leading to extensive-prolonged fishery closures, and severe economic losses. This  
27 is particularly problematic for the king scallop *Pecten maximus*, which retains high burdens of  
28 DA from months to years compared to other fast-depurator bivalves. Nonetheless, the  
29 physiological and cellular processes responsible for this retention are still unknown. In this  
30 work, for the first time, a novel immunohistochemical techniques based on the use of an anti-  
31 DA antibody was successfully developed and applied for DA-detection in bivalve tissues at a  
32 subcellular level. Our results show that in naturally contaminated *P. maximus* following a  
33 *Pseudo-nitzschia australis* outbreak, DA is visualized mainly within small membrane-  
34 bounded vesicles (1 – 2.5  $\mu\text{m}$ ) within the digestive gland cells, identified as autophagosomic  
35 structures by means of immune-electron microscopy, as well as in the mucus-producing cells,  
36 particularly those from gonad ducts and digestive tract. Trapping of DA in autophagosomes  
37 may be a key mechanism in the long retention of DA in scallops. These results and the  
38 development of DA-immunodetection are essential to provide a better understanding of the  
39 fate of DA, and further characterize DA contamination-decontamination kinetics in marine  
40 bivalves, as well as the main mechanisms involved in the long retention of this toxin in *P.*  
41 *maximus*.

42 **Keywords:** Amnesic Shellfish Poisoning, domoic acid, immunodetection, toxicokinetics,  
43 scallops, autophagosomes.

44

## 45 **1. Introduction**

46 Up to date, fifty-two bloom-forming species of diatoms of the genus *Pseudo-nitzschia* have  
47 been identified in all the oceans around the world (Lelong *et al.*, 2012; Bates *et al.*, 2018), and  
48 at least twenty-eight of these are capable of synthesizing domoic acid (DA), an extremely  
49 dangerous amnesic phycotoxin responsible for amnesic shellfish poisoning (ASP) in humans  
50 (Lundholm *et al.*, 2009; Trainer *et al.*, 2012; Zabaglo *et al.*, 2016; Basti *et al.*, 2018). This  
51 toxin is a water-soluble amino acid, which acts as a potent neurotransmitter binding to the N-  
52 methyl-D-aspartate receptors in neurons of the hippocampus. DA is a structural analog of  
53 glutamic acid, proline, and glycine, three neurotransmitters targeting the NMDA-receptors  
54 essential to memory and synaptic plasticity, exhibiting respectively a three-fold to 100 fold  
55 higher affinity (Zaman *et al.*, 1997; Lefebvre & Robertson, 2010; Zabaglo *et al.*, 2016).

56 In the last two decades, *Pseudo-nitzschia* blooms have become more intense and frequent  
57 worldwide (Lelong *et al.*, 2012; Delegrange *et al.*, 2018), affecting large exploitable  
58 populations of suspension-feeding fish and molluscs, which are the main vector of ASP toxin  
59 to higher levels of the food chain, since they can accumulate large amounts of DA in their  
60 tissues through their filter-feeding activity (Trainer *et al.*, 2012; Hallegraeff, 2017; Basti *et*  
61 *al.*, 2018). Given the toxicity of DA, and as its presence in seafood represents a potential risk  
62 for human health, several countries have successfully established monitoring programs in  
63 places where *Pseudo-nitzschia* blooms are recurrent and intense (Lelong *et al.*, 2012), and  
64 also an international sanitary threshold of 20 mg DA kg<sup>-1</sup> to regulate the maximum allowable  
65 amount of this toxin in bivalves (EFSA, 2009).

66 The rates of accumulation and depuration of DA in bivalves are species-specific and highly  
67 variable (Blanco *et al.*, 2006; Bogan *et al.*, 2007). Therefore, the incidence of toxigenic  
68 *Pseudo-nitzschia* blooms on the harvest of natural beds depends on the balance between the  
69 kinetics of assimilation and elimination of the toxin (Álvarez *et al.*, 2020; Blanco *et al.*,

70 2020). In this sense, bivalves have been broadly classified into two wide categories, rapid and  
71 slow DA detoxifiers. The former depurate the toxin within days to weeks and includes some  
72 species of mussels as *Mytilus galloprovincialis* (Blanco *et al.*, 2002), *M. edulis* (Novaczek *et*  
73 *al.*, 1992; Mafra *et al.*, 2010; Bresnan *et al.*, 2017), and *Perna canalicus* (MacKenzie *et al.*,  
74 1993), oysters such as *Crassostrea virginica* (Mafra *et al.*, 2010) and *C. gigas* (Jones *et al.*,  
75 1995), and pectinids like *Argopecten purpuratus* (Alvarez *et al.*, 2020). The slow depurators  
76 can take months to years to depurate the DA. The main examples are some commercially  
77 important bivalves like *Pecten maximus* (Blanco *et al.*, 2002; Blanco *et al.*, 2006; Bresnan *et*  
78 *al.*, 2017), *Placopecten magellanicus* (Wohlgeschaffen *et al.*, 1992; Douglas *et al.*, 1997),  
79 *Siliqua patula* (Horner *et al.*, 1993), and *Spondylus cruentus* (Ha *et al.*, 2006).

80 The king scallop *P. maximus* is a high-valuable resource in Europe, and the third most  
81 important fishery species in France, with annual catches above 60,000 tons yielding a total of  
82 87 million euros in 2017 (FAO, 2020). Nonetheless, the exploitation of this species is  
83 particularly problematic since during blooms of toxigenic *Pseudo-nitzschia* species, scallops  
84 can accumulate amounts up to ~3,000 mg DA kg<sup>-1</sup> in the digestive gland (Blanco *et al.*, 2006),  
85 and lengthy retain them, even for years, due to its extremely low depuration rates, from 0.025  
86 to 0.007 d<sup>-1</sup> (Blanco *et al.*, 2002; Blanco *et al.*, 2006). Considering the slow depuration and  
87 the risk for human health, these contamination episodes lead to extensive-prolonged fishery  
88 closures, and consequently severe economic losses.

89 More than 90% of the DA burdens are accumulated in the non-edible tissues of the scallops  
90 (Blanco *et al.*, 2006). It has been proposed that DA is mainly in “free-soluble” form in the  
91 cytoplasm of the digestive gland cells (Mauriz & Blanco, 2010), and especially in the large  
92 digestive (absorptive) cells, responsible of the intracellular digestion of the pinocytized  
93 particulate matter using a complex enzymatic equipment in *P. maximus* (Beninger & Le  
94 Pennec, 2016). Hence, the digestive cells could have a particular contribution to the high

95 accumulation of DA in the digestive gland (Blanco *et al.*, 2020). The long retention time of  
96 the toxin has been hypothesized to be due to the lack of some efficient membrane transporters  
97 in *P. maximus* (Mauriz & Blanco, 2010), or the presence of some high and low-affinity  
98 glutamate receptor as the present in the razor clam *Siliqua patula* (Trainer & Bill, 2004).  
99 Nevertheless, these hypotheses has not been confirmed yet. Despite the ecological and  
100 economic consequences associated with high accumulation of DA in scallops, the  
101 mechanisms underlying such a long retention of DA in *P. maximus* are still poorly  
102 understood. Hence, the aim of this work was to develop an immunohistochemical method to  
103 detect DA at the sub-cellular level in contaminated *P. maximus* tissues and thus decipher the  
104 subcellular mechanisms involved in its accumulation and long-retention.

## 105 **2. Materials and methods**

### 106 **2.1. Biological material and sampling**

107 Twenty adult *Pecten maximus* scallops ( $9.8 \pm 0.1$  cm shell length;  $171.5 \pm 5$  g total weight)  
108 were collected by dredging from natural beds at three different sites in the west coast of  
109 Brittany, France. Six animals were obtained from the Bay of Concarneau (CN) in November  
110 2019 ( $47^{\circ} 52' 30.07''$  N,  $3^{\circ} 55' 20.82''$  W), and seven more from Camaret-sur-Mer (CM;  $48^{\circ}$   
111  $26' 33.0096''$  N,  $4^{\circ} 35' 49.6104''$  W) in May 2021, after toxigenic *Pseudo-nitzschia* blooms.  
112 Additionally, seven scallops were collected from the Bay of Brest (BB) in December 2020  
113 ( $48^{\circ} 19' 11''$  N,  $4^{\circ} 26' 33''$  W) and used as negative controls since no ASP outbreaks had  
114 recently been documented in this area.

115 Whole soft-bodies were carefully excised from the shells. The organs were then dissected in  
116 two groups: a) digestive gland (DG), and b) rest of tissues (RT) which included the gonad, the  
117 muscle, the heart, the kidney, the foot, gills and the mantle. As mentioned above, the digestive  
118 gland accumulates up to 90% of total domoic acid (DA) burdens (Blanco *et al.*, 2020); for this  
119 reason, this organ was first carefully dissected and separated from the RT to avoid any

120 transfer of toxin between organs. Consequently, the DG was separated into three pieces for  
121 subsequent histology, toxin quantification, and transmission electron microscopy analysis, as  
122 described below. The RT section was used for histology.

## 123 **2.2. Toxin extraction and quantification by High Performance Liquid Chromatography** 124 **(HPLC)**

125 Since the digestive gland accumulates most of DA, only this tissue was used for DA  
126 quantification in this work. For all 20 individuals, DA was extracted from scallop digestive  
127 gland following the procedure described by Quilliam *et al.* (1995). Frozen samples (-20 °C)  
128 were homogenised from  $200 \pm 5$  mg of tissue in 1 mL of MeOH:MQ water (1:1, v/v) using a  
129 Laboratory Mixer Mill MM 400 system (Retsch® Fisher Scientific, Illkirch-Graffenstaden,  
130 FR) at 30 Hz/s for 10 min maintaining them in an ice bath. The extract was clarified by  
131 centrifugation at  $15,000 \times g$  for 10 min at 4 °C (Eppendorf 5427 R, Thermo Scientific, West  
132 Sussex, UK) and the supernatant was isolated. An aliquot of 200 µL was filtered through a 0.2  
133 µm nylon centrifugal filter (VWR International, Radnor, PA, USA) at 10,000 g for 5 min, at 4  
134 °C. Since there may be substantial DA degradation in aqueous solutions stored in regular  
135 freezer (Thomas *et al.*, 1998), the filtered extracts were stored in amber-glass autosampler  
136 vials (Thermo Scientific, Rockwood, TN, USA) at -20 °C for two days and analysed all at the  
137 same time.

138 All fractions obtained were analysed using a Thermo Scientific (Sunnyvale, CA, USA) HPLC  
139 System with an UV spectrophotometer Waters 996 PDA-UV detector, using a C18 reverse  
140 phase column (5 µm, 250 × 4.6 mm, Phenomenex). The separation was carried out using a  
141 mobile phase consisting of eluent A (Distilled water + 0.1 % TFA) and eluent B (ACN + 0.1  
142 % TFA) with gradient conditions from 5 to 20% ACN in 20 min at a flow rate of 1 mL min<sup>-1</sup>,  
143 with an injection volume of 20 µL. The column temperature was maintained at 40 °C. A  
144 calibration curve was generated by serial dilutions in MeOH:H<sub>2</sub>O (1:1, v/v) until

145 concentrations of 0.2, 0.5, 1.0, 2.0, 4.0 and 8  $\mu\text{g DA mL}^{-1}$  ( $r = 0.99$ ) of certified DACS-1C  
146 DA standards obtained from National Research Council (Halifax, Canada). Thereupon, DA  
147 concentration was computed by comparing the absorbance at 242 nm of the chromatographic  
148 peaks of the samples with those of the reference solutions once it was checked that the  
149 retention time and the absorbance spectrum were the same. The LODs of this HPLC-UV  
150 method ranged from 0.2 to 1 mg DA  $\text{kg}^{-1}$  tissue.

### 151 **2.3. Histology and Immunohistochemical staining of domoic acid**

152 For all 20 scallops, the piece of digestive gland dedicated to histology (DG) and the rest of the  
153 tissues (RT) were separately fixed in Davidson solution for 24 hrs (Kim *et al.*, 2006), and  
154 preserved in Ethanol 70 % at 4 °C until processing. Then, tissue samples were dehydrated in  
155 ethanol series, cleared in claral, embedded in paraffin (Paraplast Plus, Leica Biosystems,  
156 Richmond, IL, USA), thin-sectioned (4  $\mu\text{m}$ ), mounted in polysine coated glass-slides (Sigma-  
157 Aldrich, St. Louis, MO, USA) and dried overnight at 37 °C (Costa & Costa, 2012), as detailed  
158 in Table I. A series of 4 consecutive sections was performed for each samples, which were  
159 used for i) immunohistochemical detection of DA (test and negative control), ii) multichromic  
160 staining and iii) Hematoxyline/eosin staining.

161 Sections were deparaffinized and rehydrated in regressive series of ethanol before  
162 immunohistochemical staining (Table I). Following preliminary trials, the final procedure  
163 employed for immunostaining was performed as described below. An antigen retrieval step  
164 was applied in order to break potential methylene bridges formed during formalin-fixation  
165 and expose antigenic sites to allow the antibodies epitope to bind. For this, sections were  
166 placed in the Universal HIER Antigen Retrieval Reagent (abcam®, Cambridge, UK) diluted  
167 in MQ water in a ratio 1:10 (v/v), heated using a pressure cooker until full pressure for 3 min,  
168 and subsequently rinsed in washing buffer (TBS 20 mM, NaCl 150 mM, pH 7.6, with 0.025%  
169 Triton™ X-100). In order to quench endogenous peroxidase activity, samples were treated



170 with a Hydrogen Peroxide Blocking Solution (abcam®, Cambridge, UK) at room  
171 temperature, and washed in washing buffer.

172 A polyclonal primary antibody anti-DA (abcam®, Cambridge, UK) was diluted (1: 1,000) in  
173 TBS 1× with 1% BSA, applied on slides, and incubated in the dark overnight. Sections were  
174 rinsed in washing buffer and then incubated in the dark for 1h with the HRP sharped IgG  
175 Goat anti-Rabbit secondary antibody (abcam®, Cambridge, UK) diluted (1:10,000) in TBS  
176 1× with 1% BSA. Immunohistochemistry experimental conditions, as well as antibody  
177 optimization-dilutions are detailed in Table II.

178 Samples were then washed and revealed with diaminobenzidine (DAB+ Chromogen Substrate  
179 Kit, abcam®, Cambridge, UK) for 10 min in the dark. Finally, slides were rinsed in washing  
180 buffer, counterstained with hematoxylin, and mounted in Faramount Aqueous Medium  
181 (Dako®, Carpinteria, CA, USA). The complete version of the suggested  
182 immunohistochemical procedure is presented in Table I.

183 Additionally, a series of slides from the same samples were stained with a multichromic  
184 procedure according to Costa & Costa (2012). This technique consists in a combination of  
185 Alcian Blue and Periodic Acid–Schiff's for the demonstration of acid mucopolysaccharides  
186 and neutral glycoconjugates, in blue and magenta tones, respectively, Hematoxylin blueing  
187 for nuclear materials, and Picric Acid to identify proteins in yellow hues.

188 A last set of sections for both DG and RT was stained with Hematoxylin–Eosin as reference  
189 (Kim *et al.*, 2006), and mounted in DPX resin. The slides were examined under a Zeiss Axio  
190 Observer Z1 light-microscope. The digestive stages of the diverticula in the DG were  
191 classified as holding, absorptive, digestion, advanced digestion, and undergoing breakdown or  
192 regeneration, according to Mathers (1976) and Beninger & Le Pennec (2016).

193 A six-level semi-quantitative scale from 0 (absent) to 2.5 (very high) was established to assess  
194 the intensity of the chromogenic anti-DA signal present in the mucus/globose cells of  
195 different tissues, the digestive gland, and the small inclusion bodies (IBs) in the digestive cells  
196 of the scallops (Table III).

#### 197 **2.4. Transmission electron microscopy and Immunogold labeling**

198 Transmission electron microscopy (TEM) studies were necessary in order to identify the  
199 small IBs with chromogenic anti-DA signal within the cells of the digestive gland. For this  
200 purposes, three small pieces of DG ( $\sim 1 \text{ mm}^3$ ) were carefully dissected from some of the non-  
201 contaminated scallops collected in the Bay of Brest ( $n = 5$ ), used as negative controls, and  
202 some of the contaminated-scallops from Camaret-sur-Mer ( $n = 5$ ) with strongest IHC signal in  
203 the IBs within the digestive cells. Samples from scallops collected at Concarneau in 2019  
204 were not considered for these analyses since the digestive glands were not processed for TEM  
205 purposes.

206 Samples were pre-fixed in glutaraldehyde 3 % (v/v) with 0.2 M cacodylate buffer (pH 7.4)  
207 supplemented with NaCl ( $21 \text{ mg mL}^{-1}$ ) for 3 h at 4 °C, rinsed in the same buffer ( $3 \times 5 \text{ min}$ ),  
208 and subsequently post-fixed in 1% (w/v) osmium tetroxide in 0.2 M cacodylate buffer (pH  
209 7.4) for 1 h in an ice bath in the dark. Fixed specimens were rinsed in Milli-Q water  
210 ( $3 \times 5 \text{ min}$ ) and dehydrated through successive baths of ethanol. Finally, samples were  
211 embedded into Spurr's resin (Science Services, Munich, Germany). After polymerization at 60  
212 °C for 24h, semi-thin sections were cut to 800 nm thickness for quality control and then ultra-  
213 thin (ca. 70-80 nm) sections were cut for examination on a Leica EM UC6 ultramicrotome  
214 (Leica Microsystems, Germany) equipped with a 45° DiATOME diamond knife and floated  
215 on nickel grids (200 mesh).

216 Immunogold labeling was performed according to Skepper & Powell (2008) with minor  
217 modifications. Briefly, the grids were etched with drops of 4% sodium metaperiodate for 10

218 min to unmask antigenic sites on the surface of the section, rinsed three times on successive  
219 drops of MQ water, and placed on drops of 1% aqueous periodic acid for 10 min to remove  
220 eventual osmium tetroxide residue. Sections were then placed on a drop of blocking solution  
221 consisting of PBS 0.01 M, 0.01% Triton X-100, Glycine 20 mM, and 1% BSA for 10 min to  
222 reduce nonspecific binding of antibodies. The anti-DA antibody (abcam) was diluted 1:200 in  
223 blocking solution, and the sections were incubated with the primary antibody solution  
224 overnight at 4 °C in a moist chamber. After washing with blocking solution (6 × 5 min), the  
225 sections were incubated with the Goat anti-Rabbit IgG secondary antibody conjugated with 6-  
226 nm gold particles (abcam/ab41498) diluted 1:500 in blocking solution for 2 h at 28 °C, and  
227 consecutively rinsed in blocking solution and MQ water. Contrast reagents (e.g. uranyl  
228 acetate and lead citrate) were not applied to avoid masking the nanogold particles.

229 Immunogold labeling experimental conditions, as well as antibody optimization-dilutions are  
230 shown in Table II. Finally, the samples were examined under a transmission electron  
231 microscope JEOL JEM 1400 operated at 120 kV on the imaging platform of Brest University.  
232 The autophagosomal structures identified in this work by means of MET were classified  
233 according to their morphology and stage of development in marine bivalve cells (Owen, 1972;  
234 Yurchenko & Kalachev, 2019; Picot *et al.*, 2019).

## 235 **2.5. Statistical analysis**

236 To determine significant differences in toxin burdens in the digestive gland of scallops  
237 collected in the different sampling sites, *a priori* Fligner-Killeen's and Shapiro–Wilk test  
238 were used to evaluate the heterogeneity of variances and normality of frequencies of the data,  
239 respectively (Hector, 2015); the assumptions were not met. Values of DA concentrations were  
240 analyzed using a Kruskal-Wallis Test, where “the sampling site” was fixed as factor. In case  
241 of significant differences, a *post hoc* pairwise Wilcoxon rank test with Benjamini & Hochberg  
242 (BH) p-value adjustment was used to detect differences among means. For IHC results, Chi-

243 square test ( $\chi^2$ ) were applied to assess statistically significant differences in the chromogenic  
244 anti-DA signal present in each tissue of the scallops. When needed, *a posteriori* Tukey HSD  
245 test were used to identify differences between means. All the statistical analyses were  
246 performed using command lines in the R language (R v. 4.0.2, R Core Team, 2017), and  
247 graphics were generated with the R package ggplot2 on the Rstudio programming interface.  
248 All values are expressed as mean  $\pm$  standard error (SE). Differences were considered  
249 statistically significant at  $\alpha = 0.05$  for all analyses (Hector, 2015).

### 250 **3. Results**

#### 251 **3.1. Domoic acid (DA) quantification**

252 Significant differences in the amount of DA accumulated in the digestive gland (DG) of the  
253 scallops from the three sampling sites were found after toxin quantification analysis by  
254 HPLC-UV (Fig. 1). Highest burdens ( $P < 0.05$ ) of toxin were recorded in animals from  
255 Concarneau (CN) ( $446.6 \pm 101.3$  mg DA  $\text{kg}^{-1}$ ) followed by those from Camaret-sur-Mer  
256 (CM) ( $82.5 \pm 4.9$  mg DA  $\text{kg}^{-1}$ ), while the significant lowest values were detected in the  
257 scallops from the Bay of Brest (BB) ( $1.6 \pm 0.4$  mg DA  $\text{kg}^{-1}$ ).

#### 258 **3.2. Histology and immunohistochemistry (IHC)**

259 The presence of DA was detected by IHC, as brown chromogenic signal, within the tissues of  
260 all contaminated scallops (Fig. 2, 3 and 4). The absence of non-specific background staining  
261 during IHC process was confirmed in control slides incubated with the secondary antibody  
262 but without the primary anti-DA antibody (Fig. 2 A-C, Fig. 3 C, D and Fig. 4 E-H). The DA  
263 brown chromogenic signal was observed mainly throughout the DG, and readily detected in  
264 highly contaminated scallops from CN and CM. The typical DA immuno-staining observed in  
265 the DG of scallops sampled at CN and CM is illustrated in Figures 2D-F. As shown in Fig.  
266 2D, within the DG, the strongest immunoreactivity was observed in small ( $\sim 1$ - $2.5$   $\mu\text{m}$ )  
267 spherical inclusion bodies (IBs) distributed exclusively throughout the cytoplasm of the

268 digestive (absorptive) cells of the digestive diverticula, which trapped an intense chromogenic  
269 staining (Fig. 2E, F). The anti-DA chromogenic signal detected in the DG of scallops from  
270 CN and CM has the same sub-cellular localization although DA burdens were significantly  
271 different between scallops from the two locations.

272 The multichromic staining allowed to clearly identifying these IBs within the cytoplasm of  
273 the digestive cells (Fig. 2G). As observed in Fig. 2H and 2I, the IBs had a dark violet-magenta  
274 dye, indicating the presence of neutral carbohydrates and neutral glycoconjugates on their  
275 surface. The IBs did not acquire any coloration with the conventional H&E staining (Fig. 2L).  
276 No histopathological patterns were observed in the DG of the scallops, even for the highest  
277 toxin burdens (Fig. 2J, K). The overall histological evidence allowed to observe that the IBs  
278 with DA-immunoreactivity were found mainly in the digestive cells of the diverticula in  
279 stages of active digestion (Fig. 2F, H, I, K, L).

280 In the samples from significantly weakly-contaminated scallops from BB, a slight-blurred and  
281 not well-located DA-chromogenic signal was observed in the “breakdown” and  
282 “regenerating” digestive diverticula of the DG (Fig. 3A-B). Nonetheless, it was possible to  
283 localize a few IBs with immunoreactivity in the cytoplasm of the remaining digestive cells  
284 (Fig. 3B). The H&E staining also allowed corroborating the absence of histopathologies in the  
285 DG due to DA accumulation (Fig. 3E, F).

286 The DA-localization in the rest of the tissues was similar in all the scallops contaminated  
287 from ~2 up to ~750 mg DA kg<sup>-1</sup> (Fig. 4). The DA-labeling was detected only in the mucus of  
288 the epithelia that lines the outer part of the stomach (Fig. 4A), in the globose cells embedded  
289 in the epithelium of the intestine (Fig. 4B), and in the globose cells of the spawning channels  
290 or gonadic ducts in the female (Fig. 4C) and male (Fig. 4D) gonads. No DA signal was found  
291 in any other tissues such as gills, mantle, labial palps, kidneys or adductor muscle. With the

292 multichromic staining, it was possible to corroborate the presence of a light-blue coloration  
293 corresponding to acid glycoconjugates in the globose cells with immunolabeling (Fig. 4I-L).  
294 As seen in Fig. 4M-P, no histopathologies were observed in any of the additional tissues  
295 analyzed in this work.

296 As shown in Table IV, DA staining coverage in the DG was the same ( $P > 0.05$ ) for scallops  
297 from CN and CM, while the anti-DA chromogenic signal detected in the DG of the scallops  
298 collected at BB was significantly lower. On the other hand, the chromogenic signal detected  
299 in the rest of the tissues (stomach, intestine, ovary, and testicle) was not different ( $P > 0.05$ )  
300 between the strongly (CN and CM) and weakly (BB) contaminated scallops.

### 301 **3.3. Immunoelectron microscopy**

302 The IBs observed in the cytoplasm of the digestive cells in the diverticula of scallops with a  
303 dark-violet coloration by means of multichromic staining, and presenting a strong DA-  
304 immunostaining were analyzed by transmission electron microscopy (TEM) in order to  
305 decipher their cellular nature (Fig. 5). The diameter of these IBs ranged between 1-2.5  $\mu\text{m}$ .  
306 Early single-membrane-bound IBs structures (Fig. 5A) were observed frequently in the apical  
307 and sub-apical regions of the digestive cells. Meanwhile late-developed structures with a  
308 double-membrane-bound and a halo (Fig. 5B) were observed mainly in the mid-basal region  
309 of the cytoplasm, and often clustered into groups of 3-6 vesicles that may be or not  
310 surrounded by a single-membrane (Fig. 5C) and fusing with the lysosomes of the cell (Fig  
311 5D). The morphological observations by TEM described above allowed identifying these IBs  
312 as autophagic vesicles.

313 On a second hand, we coupled the use of the specific anti-DA antibody and a secondary  
314 antibody conjugated with gold nanoparticles to the TEM analyzes (immunogold labeling). As  
315 seen in Fig. 5A-D, no anti-DA signal was observed in any subcellular structure of the GD in

316 the slide incubated without anti-DA primary antibody. By means of the immunogold labeling,  
317 DA-signal was found mostly in the undigested material attached to the inner side of the  
318 membranes within early (Fig. 5E-F) and late-autophagosomes (Fig. 5G-H), while a slight  
319 signal of gold-nanoparticles corresponding to the toxin was observed in the halo of  
320 autophagosomes and in the cytoplasm of the digestive cells (Fig. 5E-H).

#### 321 **4. Discussion**

322 In this work, for the first time, immunolabeling by IHC using photonic microscopy and  
323 immunogold using TEM has been successfully used for the localization of DA at the  
324 subcellular level in naturally contaminated marine mollusc tissues. The technique set up in the  
325 present paper has been shown to work for the immunostaining of DA with high precision,  
326 either in heavily contaminated (up to 750 mg DA kg<sup>-1</sup> GD) or in weakly-contaminated  
327 scallops (~1 mg DA kg<sup>-1</sup> DG) without nonspecific labeling. Although other methods, such as  
328 HPLC-UV/MS (Quilliam *et al.*, 1989) and ELISA (Litaker *et al.*, 2008), have been widely  
329 used to quantify DA content in contaminated shellfish with a high-resolution power (0.1 – 1  
330 µg DA g<sup>-1</sup>), they do not allow the subcellular visualization of DA in the tissues, as opposed to  
331 the immunolabeling methods developed in this study. Furthermore, this immunostaining  
332 method has proven to be suitable to be coupled with TEM, allowing to pinpoint DA  
333 localization.

334 Using a subcellular fractionation analysis on homogenized DA-contaminated digestive glands  
335 of *P. maximus*, Mauriz & Blanco (2010) found that almost 90% of the toxin accumulated in  
336 this organ was in soluble form in the cytoplasm of the cells, with a mostly homogeneous  
337 distribution within the DG (Blanco *et al.* 2020). One mechanism that could influence high  
338 accumulation and long retention of DA in this species could be its binding to high affinity  
339 receptors, as those found in the razor clam *S. patula* (Trainer & Bill, 2004). Moreover, Mauriz

340 & Blanco (2010) concluded that the cause of the long DA-retention was not the binding of the  
341 toxin to some cellular component, but the lack of some efficient membrane transporters in the  
342 scallops. Our results cope with these findings, since most of the DA immune-signal was  
343 localized in the cytoplasm of the digestive cells of the digestive diverticula. Several digestive  
344 stages (holding, absorptive, digestion, advanced digestion, breakdown, and regeneration) have  
345 been described for the digestive diverticula of *P. maximus* (Mathers, 1976). In this work, the  
346 inclusion bodies (IBs) with anti-DA signal were observed mostly in the digestive cells of the  
347 diverticula in states of active digestion (absorption, digestion and advanced digestion). This is  
348 probably due to digestive cells predominate in these digestion stages and are responsible for  
349 the intracellular enzymatic digestion of the material ingested by pinocytosis (Beninger & Le  
350 Pennec, 2016). Free domoic acid in the cytoplasm was visualized by immunogold.

351 Nonetheless, the evidence of this work suggests that a significant proportion of the toxin is  
352 not simply "free-dissolved" in the cytoplasm, but is enclosed in small (1-2.5  $\mu\text{m}$ ) membrane-  
353 bound vesicles, identified as autophagosomal structures by means of TEM, distributed  
354 throughout the cytoplasm of digestive cells in digestive condition.

355 Autophagy is a well-developed, highly regulated, and complex-dynamic system related to  
356 ingestion, storage and catabolic processes of intracellular digestion (Balbi *et al.*, 2018; Wang  
357 *et al.*, 2019; Zhao *et al.*, 2021). In bivalves, autophagy plays a key role in maintaining cell  
358 homeostasis (Carella *et al.*, 2015). This mechanism has been used as an indicator of cell  
359 injury in response to different stressors (Moore, 2004; Picot *et al.*, 2019), such as  
360 environmental changes (Moore, 2008), and the innate-immune response to pathogens (Canesi  
361 *et al.*, 2002; Moreau *et al.*, 2015; Canesi *et al.*, 2016; Balbi *et al.*, 2018) However, nothing is  
362 still known on the role of autophagy in ingestion, mobilization and excretion of phycotoxins  
363 in these organisms.



364 During autophagy, cytoplasmic components, either of exogenous (e.g. contaminants, and  
365 pathogens), or endogenous (macromolecules and organelles) origin are sequestered into  
366 spherical-shaped vesicles with double membrane layers called autophagosomes.  
367 Subsequently, they are delivered to lysosomes for degradation, where the outer membrane of  
368 the autophagosome fuses with a lysosome to form an autolysosome (Cuervo, 2004; Wang *et*  
369 *al.*, 2019). Finally, the hydrolases of the lysosome degrade the autophagosome-delivered  
370 contents and its inner membrane (Zhao *et al.*, 2021).

371 In samples of DA-contaminated scallops, mostly two types of membrane-bound  
372 autophagosomic vesicles were identified by transmission electron microscopy as part of this  
373 dynamic system. Early autophagosomes, which are usually involved in the ingestion and  
374 accumulation of exogenous materials, were present mainly in the apical region of the  
375 digestive cells; whereas in the mid- and basal regions of the cytoplasm we observed late-  
376 autophagosomes. These autophagosomes are involved in digestion and accumulation of  
377 undigested and indigestible residues, which may then be stored within the cell or eliminated  
378 (Owen, 1972; Zhao *et al.*, 2021). The transformation rate from early to late-autophagosomes  
379 is presumably dependent on the nature of the ingested material, and variations of this basic  
380 but highly-complex cycle probably depends on feeding rates, nature of the ingested  
381 food/substances, and the mode of release/excretion of the autophagosomic vesicles (Owen,  
382 1972; Cuervo, 2004). The processing of autophagosomes by intracellular digestion could be a  
383 key to explain the long retention time of DA in the digestive cells of *P. maximus*. The toxin is  
384 probably normally ingested and accumulated in early autophagosomes, but cannot then be  
385 digested by the lysosomal machinery, thus remaining stored within autophagosomes as  
386 indigestible material in the cytoplasm of the cells. Moreover, it is difficult to know exactly  
387 how long it may take for the material present within autophagosomes to be excreted; since

388 some experiments suggest that it can go from a few minutes to indefinite periods of time  
389 (Owen, 1972; Cuervo, 2004).

390 After DA injection in the adductor muscle, and subsequent transcriptomic analysis of the  
391 digestive gland of *P. maximus*, Ventoso *et al.* (2021) found as well as an upregulation of  
392 genes related to autophagy and vesicle-mediated transport. Even though these results were not  
393 obtained under conditions of ingestion of the toxin through the filtration of toxic *Pseudo-*  
394 *nitzschia* cells, these findings could also indicate that the formation of autophagosomic  
395 structures could be part of explanation for DA long retention, blocking its digestion and  
396 excretion.

397 In order to corroborate whether autophagy is the subcellular mechanism involved in the long  
398 retention of DA in the DG of *P. maximus*, the next step would be to follow, by means of  
399 digital image analysis, the evolution of the anti-DA chromogenic signal in the tissues in  
400 parallel to the formation of autophagosomes with strong DA-immunoreactivity within the  
401 digestive cells during the contamination and decontamination processes.

402 There is evidence of the profound interspecific differences in the retention and depuration of  
403 DA in bivalves, even between pectinid species, like for example *P. maximus* and *A.*  
404 *purpuratus*. While the former is capable of accumulating up to 3,000 mg DA kg<sup>-1</sup> and retain it  
405 for months or even years (Blanco *et al.*, 2006), *A. purpuratus* transfers almost all the DA  
406 accumulated in the digestive gland to other organs (mainly the intestine and the gonad) within  
407 a few days and then excrete the toxin into the environment (Álvarez *et al.*, 2020). Although  
408 the physiological mechanisms enabling *A. purpuratus* to quickly depurate the DA are  
409 unknown, Alvarez *et al.* (2020) hypothesized a two-compartment model, where the toxin  
410 acquired by the DG is quickly transported to other organs. In *P. maximus*, we could  
411 hypothesized that a significant part of DA accumulated stay in DG due to the absence of

412 specific transporter as proposed by Mauriz and Blanco (2020), and that, secondly, its its  
413 detoxification be slower due to the formation of autophagosomes that retain the DA. Further  
414 analyses, comparing these species, using histological, immunohistochemistry, as well as  
415 molecular biology techniques appear necessary to confirm this hypothesis and to determine  
416 whether autophagy appears in other slow-depurator shellfish species.

417 In the rest of the tissues of *P. maximus*, the IHC technique developed in this work revealed  
418 specific toxin-immunoreactivity and thus DA-localization within the mucus, particularly in  
419 the mucocytes of some epithelia such as the stomach and intestine, and in the mucocytes of  
420 the gonad spawning-ducts. Mucus is composed of water, glycoproteins and mineral salts  
421 (Davies & Hawkins, 1998), and is produced by almost all the epithelia of mollusks, playing  
422 an essential role in several functions such as lubrication, nutrition, the first barrier against  
423 environmental stress, and as an innate-immune barrier against pathogenic infections (Allam &  
424 Pales Espinosa, 2015). Hence, complementary studies are necessary to determine if DA has  
425 an affinity or is chemically-bounded to any of the components of mucus, and if the latter may  
426 be involved in DA-depuration or retention in the scallops. This hypothesis is totally new,  
427 since DA detection techniques in contaminated bivalve tissues had never allowed to localize  
428 the toxin at the level of mucus or mucus-producing cells during a contamination and  
429 decontamination scenario.

## 430 **5. Conclusions**

431 The DA-immunodetection methods proposed in this work by immunohistochemistry and  
432 immunogold are innovative ways to visualize the phycotoxin DA in the tissues of the king  
433 scallop *P. maximus*, and to decipher the subcellular mechanism involved in the retention of  
434 this toxin in a marine bivalve. The results of this work show that, most of the DA is found in  
435 the cytoplasm of digestive cells of *P. maximus*, as previously mentioned by Mauriz & Blanco

436 (2010). Notwithstanding, most part of DA-signal does not appear free in the cytoplasm, but  
437 mainly within autophagic structures as revealed by DA-immunostaining, suggesting that  
438 autophagic subcellular mechanisms could play a crucial role in the retention of the ASP toxin  
439 in the digestive cells of scallops. Furthermore, the role of mucus in the retention-depuration of  
440 DA in *P. maximus* must be investigated, since the toxin was only immunolocalized in the  
441 mucus of specific remaining tissues.

442 DA-immunodetection also provides a great tool to compare DA-localisation within species  
443 depurating at different speed over a contamination and decontamination period. The findings  
444 of this work constitute an important step forward in explaining the slow depuration of DA in  
445 *P. maximus*, and provide basic knowledge for the proposal of procedures to accelerate the  
446 depuration of the toxin in this species.

#### 447 **Acknowledgments**

448 The authors are grateful to Aouregan Terre-Terrillon and Erwan Amice for the scallop  
449 sampling. We thank Nelly Le Goïc and Adeline Bidault (from IUEM-LEMAR, Brest) for  
450 their technical support. We also thank Amélie Derrien and Malwenn Lassudrie (Ifremer,  
451 Concarneau) for their valuable help with HPLC technique, as well as Philippe Elies (PIMM  
452 platform, UBO, Brest) for his assistance with transmission electron microscopy.

#### 453 **Conflict of interest**

454 All authors approved the final version of this manuscript and declare no conflict of interest.

#### 455 **Funding**

457 This work received financial support from the research project “MaSCoET” (Maintien du  
458 Stock de Coquillages en lien avec la problématique des Efflorescences Toxiques) financed by  
459 France Filière Pêche and Brest Métropole, and the project “CoDDA” (Contamination and  
460 Decontamination of Domoic Acid in marine bivalves) funded by ISblue under the academic

461 responsibility of JLGC, CF and HH. JLGC is recipient of a doctorate fellowship from  
462 CONACyT, Mexico (REF: 2019-000025-01EXTF-00067).

### 463 **Data availability statement**

464 The evidence and data that support the findings of this study are available from the  
465 corresponding author upon reasonable request.

### 466 **Ethics statements**

467 The adult scallops (*Pecten maximus*) were transported and handled according to the  
468 International Standards for the Care and Use of Laboratory Animals. The number of sampled  
469 organisms contemplated "the rule of maximizing information published and minimizing  
470 unnecessary studies". In this sense, 20 scallops were considered as the minimum number of  
471 organisms needed for this work.

### 472 473 **Literature cited**

474 Allam, B., & Pales Espinosa, E. (2016). Bivalve immunity and response to infections: Are we  
475 looking at the right place? *Fish & Shellfish Immunology*, 53, 4–12.

476 <https://doi.org/10.1016/j.fsi.2016.03.037>

477 Álvarez, G., Rengel, J., Araya, M., Álvarez, F., Pino, R., Uribe, E., Díaz, P.A., Rossignoli,  
478 A.E., López-Rivera, A., & Blanco, J. (2020). Rapid Domoic Acid Depuration in the Scallop  
479 *Argopecten purpuratus* and Its Transfer from the Digestive Gland to Other Organs. *Toxins*,  
480 12, 698. <https://doi.org/10.3390/toxins12110698>

481 Balbi, T., Cortese, K., Ciacci, C., Bellese, G., Vezzulli, L., Pruzzo, C., & Canesi, L. (2018).  
482 Autophagic processes in *Mytilus galloprovincialis* hemocytes: effects of *Vibrio tapetis*. *Fish*  
483 *& Shellfish Immunology*, 73, 66–74. <https://doi.org/10.1016/j.fsi.2017.12.003>

484 Basti, L., Hegaret, H., & Shumway, S.E. (2018). Harmful Algal Blooms and Shellfish. In  
485 Shumway, S.E., Burkholder, J.M., Morton, S.L., eds. Harmful Algal Blooms a Compendium  
486 Desk Reference, pp.135–191. John Wiley & Sons Inc., Hoboken, NJ.

487 Bates, S. S., Hubbard, K. A., Lundholm, N., Montresor, M., & Leaw, C. P. (2018). *Pseudo-*  
488 *nitzschia*, *Nitzschia*, and domoic acid: New research since 2011. *Harmful Algae*,  
489 <http://dx.doi.org/10.1016/j.hal.2018.06.001>

490 Blanco, J., Acosta, C. P., Mariño, C., Muñoz, S., Martín, H., Moroño, Á., Correa, J., Arévalo,  
491 F. & Salgado, C. (2006). Depuration of domoic acid from different body compartments of the  
492 king scallop *Pecten maximus* grown in raft culture and natural bed. *Aquatic Living Resources*,  
493 19(3), 257–265. <http://dx.doi.org/10.1051/alr:2006026>

494 Blanco, J., Acosta, C., Bermúdez de la Puente, M., & Salgado, C. (2002). Depuration and  
495 anatomical distribution of the amnesic shellfish poisoning (ASP) toxin domoic acid in the  
496 king scallop *Pecten maximus*. *Aquatic Toxicology*, 60(1-2), 111–121.  
497 [http://dx.doi.org/10.1016/s0166-445x\(01\)00274-0](http://dx.doi.org/10.1016/s0166-445x(01)00274-0)

498 Blanco, J., Mauríz, A. & Álvarez, G. (2020). Distribution of Domoic Acid in the Digestive  
499 Gland of the King Scallop *Pecten maximus*. *Toxins*, 12(371), 1-11.  
500 <http://dx.doi.org/10.3390/toxins12060371>

501 Bogan, Y.M., Harkin, A.L., Gillespie, J., Kennedy, D.J., Hess, P., & Slater, J.W. (2007). The  
502 influence of size on domoic acid concentration in king scallop, *Pecten maximus* (L.). *Harmful*  
503 *Algae*, 6, 15–28. <https://doi.org/10.1016/j.hal.2006.05.005>

504 Bresnan, E., Fryer, R. J., Fraser, S., Smith, N., Stobo, L., Brown, N., & Turrell, E. (2017).  
505 The relationship between *Pseudo-nitzschia* (Peragallo) and domoic acid in Scottish shellfish.  
506 *Harmful Algae*, 63, 193–202. <https://doi.org/10.1016/j.hal.2017.01.004>

507 Beninger, P. G., & Le Pennec, M. (2016). Structure and function in scallops. In S. E.  
508 Shumway, & G. J. Parsons (Eds.), *Scallops: Biology, ecology, aquaculture, and fisheries* (pp.  
509 85–159). Elsevier.

510 Canesi, L., Ciacci, C., & Balbi, T. (2016). Invertebrate Models for Investigating the Impact of  
511 Nanomaterials on Innate Immunity: The Example of the Marine Mussel *Mytilus* spp. *Current*  
512 *Bionanotechnology*, 2(2), 77-83. <https://doi.org/10.2174/2213529402666160601102529>

513 Canesi, L., Gallo, G., Gavioli, M., & Pruzzo, C. (2002). Bacteria-hemocyte interactions and  
514 phagocytosis in marine bivalves. *Microscopy Research and Technique*, 57(6), 469–476.  
515 <https://doi.org/10.1002/jemt.10100>

516 Carella, F., Feist, S., Bignell, J., & De Vico, G. (2015). Comparative pathology in bivalves:  
517 aetiological agents and disease processes. *Journal of Invertebrate Pathology*, 131, 107–120.  
518 <https://doi.org/10.1016/j.jip.2015.07.012>

519 Costa, P. & Costa, M.H. (2012). Development and application of a novel histological  
520 multichrome technique for clam histopathology. *Journal of Invertebrate Pathology*, 110, 411-  
521 414. <http://dx.doi.org/10.1016/j.jip.2012.04.013>

522 Cuervo, A. M. (2004). Autophagy: Many paths to the same end. *Molecular and Cellular*  
523 *Biochemistry*, 263(1/2), 55–72. <https://doi.org/10.1023/b:mcbi.0000041848.57020.57>

524 Davies, M.S. & Hawkins, S.J. (1998). Mucus from Marine Molluscs. pp. 1–71. In: Blaxter  
525 J.H.S., Southward A.J., & Tyler P.A. (eds), *Advances in Marine Biology*, Academic Press.

526 Delegrange, A., Lefebvre, A., Gohin, F., Courcot, L., & Vincent, D. (2018). *Pseudo-nitzschia*  
527 *sp.* diversity and seasonality in the southern North Sea, domoic acid levels and associated  
528 phytoplankton communities. *Estuarine, Coastal and Shelf Science*, 214, 194–206.  
529 <https://doi.org/10.1016/j.ecss.2018.09.030>

530 Douglas, D. J., Kenchington, E. R., Bird, C. J., Pocklington, R., Bradford, B., & Silvert, W.  
531 (1997). Accumulation of domoic acid by the sea scallop (*Placopecten magellanicus*) fed  
532 cultured cells of toxic *Pseudo-nitzschia multiseriata*. *Canadian Journal of Fisheries and*  
533 *Aquatic Sciences*, 54(4), 907–913. <https://doi.org/10.1139/f96-333>

534 EFSA. (2009). Panel on Contaminants in the Food Chain. Scientific Opinion of the Panel on  
535 Contaminants in the Food Chain on a request from the European Commission on marine  
536 biotoxins in shellfish—Domoic acid. *EFSA J.*, 1181, 1–61.

537 FAO. 2020. The State of World Fisheries and Aquaculture 2020. Sustainability in action.  
538 Rome. <https://doi.org/10.4060/ca9229en>

539 Ha, D. V., Takata, Y., Sato, S., Fukuyo, Y., & Kodama, M. (2006). Domoic acid in a bivalve  
540 *Spondylus cruentus* in Nha Trang Bay, Khanh Hoa Province, Vietnam. *Coastal Marine*  
541 *Science*, 30(1), 130–132.

542 Hallegraef, G.M. (2017). Marine phycotoxins and seafood safety. In: Witczak, A., Sikorski,  
543 Z.E. (Eds.), *Toxins and Other Harmful Compounds in Foods*. CRC Press, Taylor & Francis  
544 Group, Boca Raton, Florida, pp. 63–84.

545 Hector, A. (2015). *The new statistics with R: an introduction for biologists* (1st ed.). New  
546 York, Oxford University Press.

547 Horner, R.A., Kusske, M.B., Moynihan, B.P., Skinner, R.N. & Wekell, J.C. (1993). Retention  
548 of Domoic Acid by Pacific Razor Clams, *Siliqua patula* (Dixon, 1789): Preliminary Study.  
549 *Journal of Shellfish Research*, 12, 451-456.

550 Jones, T. O., Whyte, J. N. C., Ginther, N. G., Townsend, L. D., & Iwama, G. K. (1995).  
551 Haemocyte changes in the pacific oyster, *Crassostrea gigas*, caused by exposure to domoic  
552 acid in the diatom *Pseudonitzschia pungens f. multiseriis*. *Toxicon*, 33(3), 347–353.  
553 [https://doi.org/10.1016/0041-0101\(94\)00170-](https://doi.org/10.1016/0041-0101(94)00170-)

554 Kim, Y., Ashton-Alcox, K.A. & Powell, E.N. (2006). *Histological Techniques for Marine*  
555 *Bivalve Molluscs: update*. NOAA Technical Memorandum NOS NCCOS 27, Maryland.

556 Lefebvre, K. A., & Robertson, A. (2010). Domoic acid and human exposure risks: A review.  
557 *Toxicon*, 56(2), 218–230. <http://dx.doi.org/10.1016/j.toxicon.2009.05>

558 Lelong, A., Hégaret, H., Soudant, P., & Bates, S. S. (2012). *Pseudo-nitzschia*  
559 (Bacillariophyceae) species, domoic acid and amnesic shellfish poisoning: revisiting previous  
560 paradigms. *Phycologia*, 51(2), 168–216. <http://dx.doi.org/10.2216/11-37.1>

561 Litaker, R. W., Stewart, T. N., Eberhart, B.-T. L., Wekell, J. C., Trainer, V. L., Kudela, R. M.,  
562 Miller, P.E., Roberts, A., Hertz, C., Johnson, T.A., Frankfurter, G., Smith, G.J., Schnetzer, A.,  
563 Schumacker, J., Bastian, J.L., Odell, A., Gentien, P., Le Gal, D., Hardison, D.R., & Tester, P.  
564 A. (2008). Rapid Enzyme-linked Immunosorbent Assay for Detection of the Algal Toxin  
565 Domoic Acid. *Journal of Shellfish Research*, 27(5), 1301–1310. [https://doi.org/10.2983/0730-](https://doi.org/10.2983/0730-8000-27.5.1301)  
566 [8000-27.5.1301](https://doi.org/10.2983/0730-8000-27.5.1301)

567 Lundholm, N., Churro, C., Fraga, S., Hoppenrath, M., Iwataki, M., Larsen, J., Mertens, K.,  
568 Moestrup, Ø., & Zingone, A. (Eds) (2009 onwards). *IOC-UNESCO Taxonomic Reference*  
569 *List of Harmful Micro Algae*. Accessed at <https://www.marinespecies.org/hab> on 2022-02-20.  
570 <https://doi.org/10.14284/362>

571 Mackenzie, A.L., White, D.A., Sim, P.G., & Holland, A.J. (1993). Domoic acid and the New  
572 Zealand greenshell mussel (*Perna canaliculus*). In: Smayda, T.J., Shimizu, Y. (Eds.), *Toxic*  
573 *Phytoplankton Blooms in the Sea*. Elsevier Science Publishers, pp. 607–612.



574 Mafra, L. L., Bricelj, V. M., & Fennel, K. (2010). Domoic acid uptake and elimination  
575 kinetics in oysters and mussels in relation to body size and anatomical distribution of toxin.  
576 *Aquatic Toxicology*, 100(1), 17–29. <https://doi.org/10.1016/j.aquatox.2010.07.0>

577 Mathers, N. F. (1976). The effects of tidal currents on the rhythm of feeding and digestion in  
578 *Pecten maximus* L. *Journal of Experimental Marine Biology and Ecology*, 24(3), 271-283.  
579 [https://doi.org/10.1016/0022-0981\(76\)90059-9](https://doi.org/10.1016/0022-0981(76)90059-9)

580 Mauriz, A., & Blanco, J. (2010). Distribution and linkage of domoic acid (amnesic shellfish  
581 poisoning toxins) in subcellular fractions of the digestive gland of the scallop *Pecten*  
582 *maximus*. *Toxicon*, 55(2-3), 606–611. <https://doi.org/10.1016/j.toxicon.2009.10>.

583 Moore, M. N. (2004). Diet restriction induced autophagy: A lysosomal protective system  
584 against oxidative- and pollutant-stress and cell injury. *Marine Environmental Research*, 58(2-  
585 5), 603–607. <https://doi.org/10.1016/j.marenvres.2004.03>

586 Moore, M. N. (2008). Autophagy as a second level protective process in conferring resistance  
587 to environmentally-induced oxidative stress. *Autophagy*, 4(2), 254–256.  
588 <https://doi.org/10.4161/auto.5528>

589 Moreau, P., Moreau, K., Segarra, A., Tourbiez, D., Travers, M.-A., Rubinsztein, D. &  
590 Renault, T. (2015). Autophagy plays an important role in protecting Pacific oysters from  
591 OsHV-1 and *Vibrio aestuarianus* infections. *Autophagy*, 11, 516–526.  
592 <https://doi.org/10.1080/15548627.2015.1017188>

593 Novaczek, I., Madhyastha, M. S., Ablett, R. F., Donald, A., Johnson, G., Nijjar, M. S., &  
594 Sims, D. E. (1992). Depuration of Domoic Acid from Live Blue Mussels (*Mytilus edulis*).  
595 *Canadian Journal of Fisheries and Aquatic Sciences*, 49(2), 312–318.  
596 <https://doi.org/10.1139/f92-035>

597 Owen, G. (1972). Lysosomes, peroxisomes and bivalves. *Science Progress*, 60(239), 299–  
598 318.

599 Picot, S., Morga, B., Faury, N., Chollet, B., Dégremont, L., Travers, M.-A., Renault, T. &  
600 Arzul, I. (2019). A study of autophagy in hemocytes of the Pacific oyster, *Crassostrea gigas*.  
601 *Autophagy*, 1–9. <https://doi.org/10.1080/15548627.2019.1596>

602 Quilliam, M. A., Sim, P. G., McCulloch, A. W., & McInnes, A. G. (1989). High-Performance  
603 Liquid Chromatography of Domoic Acid, a Marine Neurotoxin, with Application to Shellfish

604 and Plankton. *International Journal of Environmental Analytical Chemistry*, 36(3), 139–154.  
605 <https://doi.org/10.1080/03067318908026867>

606 R Core Team (2018). R: A language and environment for statistical computing. R Foundation  
607 for Statistical Computing, Vienna, Austria. URL <https://www.R-project.org/>.

608 Skepper, J.N. & Powell, J.M. (2008). Immunogold Staining of Epoxy Resin Sections for  
609 Transmission Electron Microscopy (TEM). *CSH Protocols*, 3(6), 1-4.  
610 <http://dx.doi.org/10.1101/pdb.prot5015>

611 Trainer, V. L., Bates, S. S., Lundholm, N., Thessen, A. E., Cochlan, W. P., Adams, N. G., &  
612 Trick, C. G. (2012). *Pseudo-nitzschia* physiological ecology, phylogeny, toxicity, monitoring  
613 and impacts on ecosystem health. *Harmful Algae*, 14, 271–300.  
614 <http://dx.doi.org/doi:10.1016/j.hal.2011.10.025>

615 Trainer, V.L. & Bill, B.D. (2004). Characterization of a domoic acid binding site from Pacific  
616 razor clam. *Aquatic Toxicology*, 69, 125–132.  
617 <http://dx.doi.org/10.1016/j.aquatox.2004.04.012>

618 Thomas, K. M., LeBlanc, D. M., & Quilliam, M. A. (1998). The 112<sup>th</sup> AOAC International  
619 Annual Meeting and Exposition, AOAC, Montreal.

620 Ventoso, P., Pazos, A.J., Blanco, J., Pérez-Parallé, M.L., Triviño, J.C., & Sánchez, J.L.  
621 (2021). Transcriptional Response in the Digestive Gland of the King Scallop (*Pecten*  
622 *maximus*) After the Injection of Domoic Acid. *Toxins*, 13, 339.  
623 <https://doi.org/10.3390/toxins13050339>

624 Wang, L., Ye, X., & Zhao, T. (2019). The physiological roles of autophagy in the mammalian  
625 life cycle. *Biological Reviews*, 94, 503–516. <https://doi.org/10.1111/brv.12464>

626 Wohlgeschaffen, G. D., Mann, K. H., Subba Rao, D. V., & Pocklington, R. (1992). Dynamics  
627 of the phycotoxin domoic acid: accumulation and excretion in two commercially important  
628 bivalves. *Journal of Applied Phycology*, 4(4), 297–310. <https://doi.org/10.1007/bf02185786>

629 Yurchenko, O., & Kalachev, A. (2019). Morphology of nutrient storage cells in the gonadal  
630 area of the Pacific oyster, *Crassostrea gigas* (Thunberg, 1793). *Tissue Cell* 56, 7–13.  
631 <https://doi.org/10.1016/j.tice.2018.11.004>

632 Zabaglo, K., Chrapusta, E., Bober, B., Kaminski, A., Adamski, M., & Bialczyk, J. (2016).  
633 Environmental roles and biological activity of domoic acid: A review. *Algal Research*, 13,  
634 94–101. <http://dx.doi.org/10.1016/j.algal.2015.11.020>

635 Zaman, L., Arakawa, O., Shimosu, A., Onoue, Y., Nishio, S., Shida, Y., & Noguchi, T.  
636 (1997). Two new isomers of domoic acid from a red alga, *Chondria armata*. *Toxicon*, 35(2),  
637 205-212. [https://doi.org/10.1016/S0041-0101\(96\)00123-7](https://doi.org/10.1016/S0041-0101(96)00123-7)

638 Zhao, Y. G., Codogno, P., & Zhang, H. (2021). Machinery, regulation and pathophysiological  
639 implications of autophagosome maturation. *Nature Reviews Molecular Cell Biology*.  
640 <http://dx.doi.org/10.1038/s41580-021-00392-4>

641 **Table I.** Full stepwise sequence of the immunohistochemical staining method.

<b>Step</b>	<b>Reagent/Solution</b>	<b>Duration</b>	<b>Temperature</b>
<i>Tissue processing</i>			
Fixation	Davidson solution	24 to 48 h	~ 4 °C
Preservation	Ethanol 70%	Days/ months	~ 4 °C
Dehydration	Ethanol 80%, 95% and 100%	8 × 1 h	~ 20 °C
Clarifying	Claral	2 × 1 h	~ 20 °C
Impregnation	Paraffin	Overnight	~ 60 °C
<i>Staining</i>			
Deparaffinization	Claral	2 × 3 min	~ 20 °C
Hydration	Ethanol 100%, 95% and 80%	5 × 3 min	~ 20 °C
Antigen retrieval	Universal HIER reagent 1×	3 min	~ 120 °C
Wash	Washing buffer <sup>a</sup>	3 × 5 min	~ 20 °C
Peroxidase quenching	Blocking peroxidase solution	2 h	~ 20 °C
Wash	Washing buffer	2 × 5 min	~ 20 °C
1st immune-staining	Primary Ab anti-DA	Overnight	~ 4 °C
Wash	Washing buffer	2 × 5 min	~ 20 °C
2nd immune-staining	Secondary Ab HRP conjugated	1 h	~ 37 °C
Wash	Washing buffer	2 × 5 min	~ 20 °C
Revelation	DAB+ substrate	10 min	~ 20 °C
Wash	Washing buffer	2 × 5 min	~ 20 °C
Counterstaining	Hematoxylin	1 min	~ 20 °C
Rinse	Tap water	A few dips	~ 20 °C

642 <sup>a</sup>TBS is recommended over PBS in washing buffer to get a cleaner background. 0.025% Triton  
 643 X-100 in the TBS reduces surface tension, allowing reagents to cover the tissue section easily.  
 644 Ab = antibody

645  
 646  
 647 **Table II.** Antibody (Ab) optimization and immunohistochemical experimental conditions.

<b>Conditions</b>	<b>Concentrations</b>		<b>Antigen retrieval<sup>a</sup></b>	<b>Peroxidase Quenching<sup>b</sup></b>
	<i>Primary Ab</i> Anti-DA	<i>Secondary Ab</i> HRP/nanogold conjugated		
<i>IHC</i>				
Negative control	Without	1: 10,000	Yes	Yes
Treated	1:1,000	1: 10,000	Yes	Yes
<i>Immunogold</i>				
Negative control	Without	1: 500	No	No
Treated	1:200	1: 500	No	No

648 <sup>a</sup>Antigen retrieval allows to break potential methylene bridges formed during formalin-fixation  
 649 and expose antigenic sites to allow the antibodies epitope to bind.

650 <sup>b</sup>Endogenous peroxidase blocking is necessary to avoid non-specific staining.

651

652 **Table III.** Semi-quantitative scale categorizing the intensity of chromogenic anti-DA signal  
 653 observed on the IHC slides.

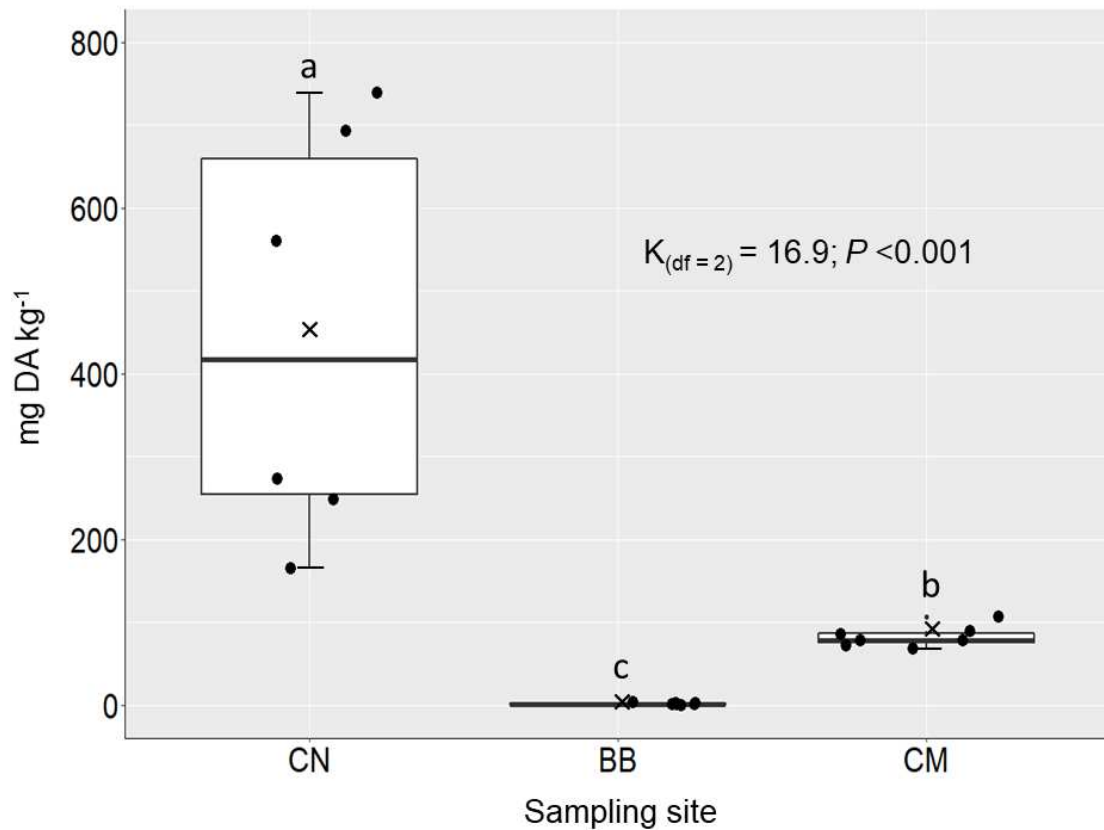
Level intensity	Occurrence of the chromogenic anti-DA staining in the examined tissue area
0	Absence
0.5	Very low (<5 occurrence/presence in all fields at magnification 10×)
1	Low (>5 occurrence/presence in all fields at magnification 10×)
1.5	Moderate (presence in all fields at magnification 20×/ covering about one tenth of the tissue area)
2	High (presence in all fields at magnification 40×/ covering about one fifth of the tissue area)
2.5	Very high (presence in all fields at magnification 60×/ covering about one-third or above of the tissue area)

654

655 **Table IV.** Comparison of IHC staining intensity of DA in the tissues of the scallops *P.*  
 656 *maximus* naturally contaminated and collected at three sites (CN = Concarneau [n = 6], BB =  
 657 Bay of Brest [n = 7], and CM = Camaret-sur-mer [n = 7]) of the northwest coast of France  
 658 between 2019 and 2021. NA: not available (not enough data), “—”: no chromogenic anti-DA  
 659 staining.

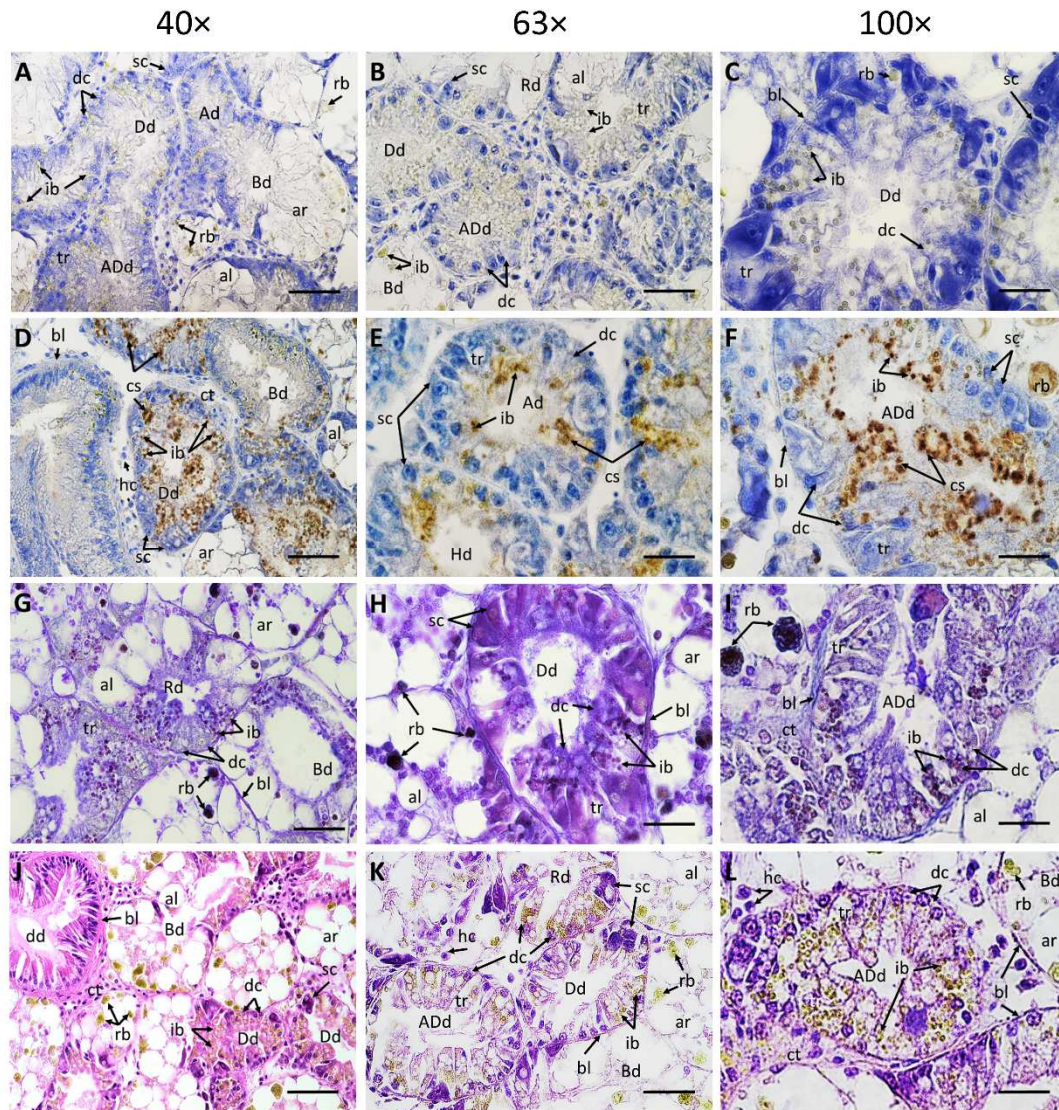
Tissue	Sampling site			Statistical analysis	
	CN	BB	CM	$\chi^2, n$	<i>p</i>
Digestive gland	2.4 ± 0.08 <sup>a</sup>	0.57 ± 0.13 <sup>b</sup>	2.4 ± 0.09 <sup>a</sup>	20.4, 20	<0.05
Stomach	1.2 ± 0.11 <sup>a</sup>	0.93 ± 0.14 <sup>a</sup>	1.3 ± 0.1 <sup>a</sup>	5.9, 20	>0.05
Intestine	1.3 ± 0.1 <sup>a</sup>	1.07 ± 0.17 <sup>a</sup>	1.3 ± 0.1 <sup>a</sup>	4.3, 20	>0.05
Ovary	1.2 ± 0.1 <sup>a</sup>	0.93 ± 0.13 <sup>a</sup>	1.3 ± 0.1 <sup>a</sup>	5.8, 20	>0.05
Testicle	1.1 ± 0.09 <sup>a</sup>	1 ± 0.15 <sup>a</sup>	1.4 ± 0.09 <sup>a</sup>	4.2, 20	>0.05
Gills	—	—	—		NA
Adductor muscle	—	—	—		NA
Mantle	—	—	—		NA
Labial palps	—	—	—		NA

660 Data (mean ± SE) were analyzed according to the sampling sites (three levels) in a Chi-square  
 661 test ( $\chi^2$ ). The  $\chi^2$  test statistic and sample size (*n*) are reported. Different superscript letters  
 662 denote statistically significant differences at *p* < 0.05.



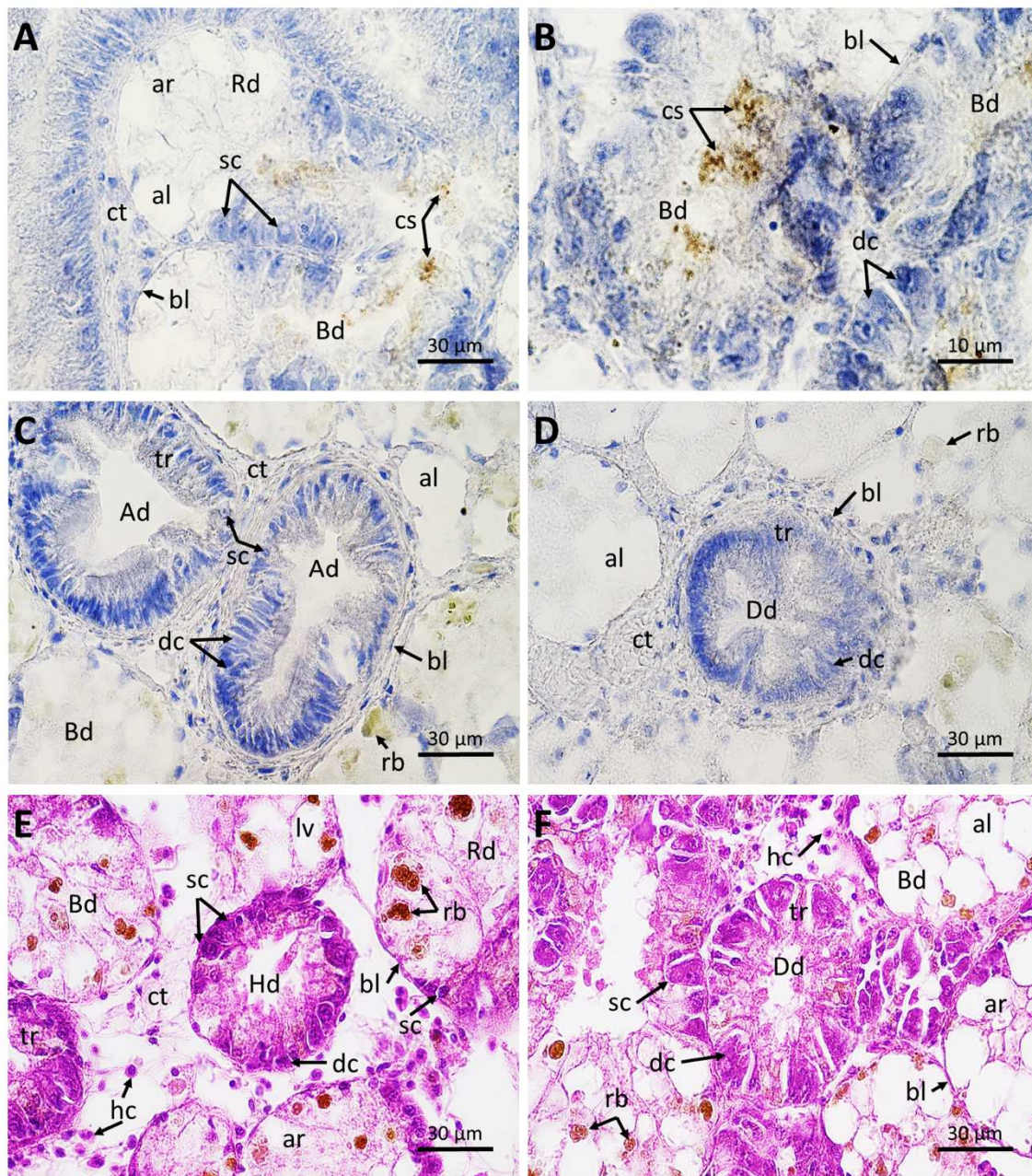
663  
664

665 **Figure 1.** DA concentrations in the digestive gland of the scallops *P. maximus* naturally  
 666 contaminated during outbreaks of the toxic *Pseudo-nitzschia* spp. and collected at three sites  
 667 (CN = Concarneau [n = 6], BB = Bay of Brest [n = 7], and CM = Camaret-sur-mer [n = 7]) of  
 668 the northwest coast of France between 2019 and 2021. The upper and lower limits of the boxes  
 669 are the quartiles, the middle horizontal line is the median, the extremes of the vertical lines are  
 670 the upper and lower limits of the observations, the dots are the individual observations, and the  
 671 crosses are the means. Data were analyzed using the sampling sites (three levels) as independent  
 672 variables in a Kruskal-Wallis Test. The K-test statistic and degrees of freedom (df) are reported.  
 673 Different superscript letters denote statistically significant differences between groups of  
 674 scallops. The level of statistical significance was set at  $\alpha = 0.05$ .



675

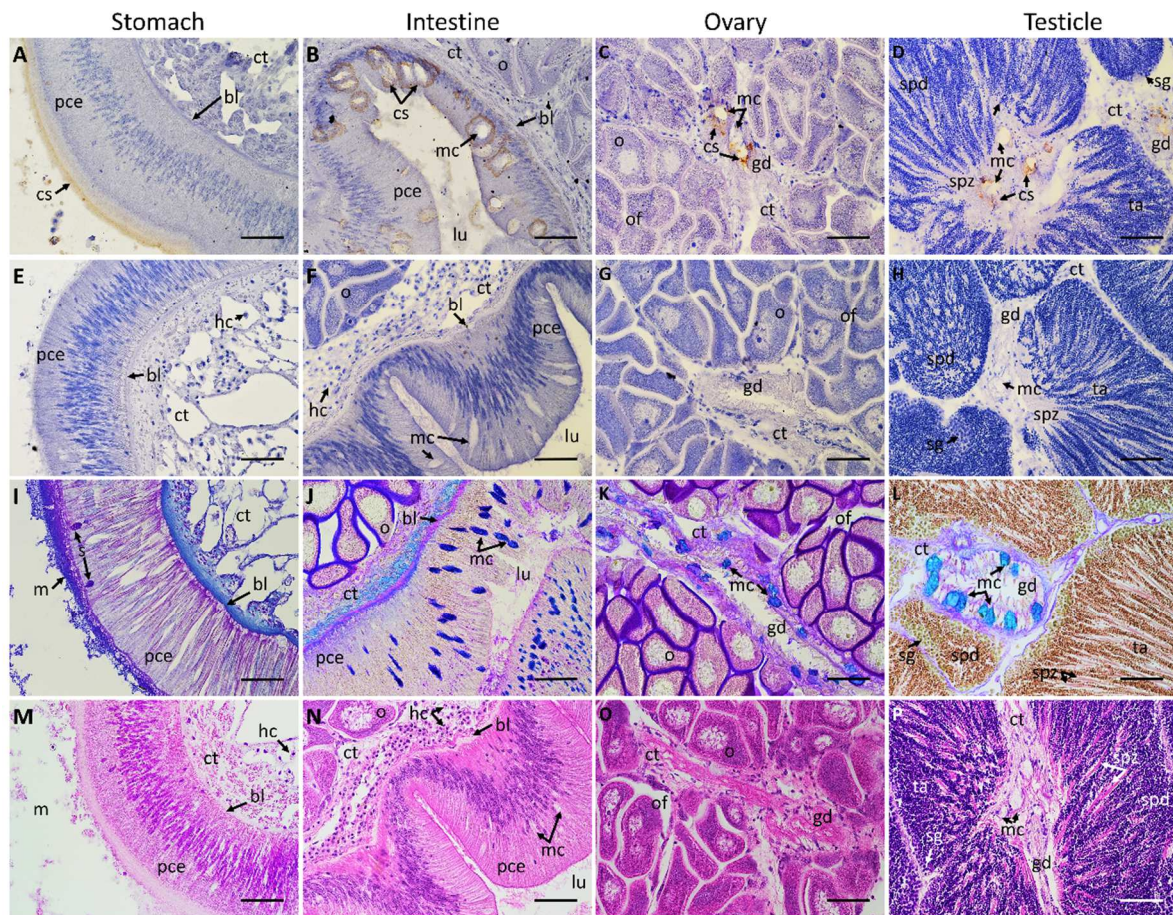
676 **Figure 2.** Microphotographs of digestive glands of scallops *P. maximus* naturally highly  
677 contaminated ( $\sim 60$  to  $750 \text{ mg DA kg}^{-1}$ ) collected at Camaret-sur-mer ( $n = 7$ ) and Concarneau  
678 ( $n = 6$ ) in the northwest coast of France between 2019 and 2021 during outbreaks of the toxic  
679 *Pseudo-nitzschia* spp. (A-C) negative controls of the IHC staining incubated with the  
680 secondary antibody but without the primary anti-DA antibody (1: 10,000 and 1: 0,  
681 respectively); (D-F) specific anti-DA immunohistochemical (IHC) staining incubated with  
682 the primary and secondary antibodies (1: 1,000 and 1: 10,000, respectively); (G-I)  
683 multichromic histochemical staining for the demonstration of neutral carbohydrates (violet-  
684 magenta dyes), acid glycoconjugates (blue hues), and proteins (yellowish tones); (J-L)  
685 conventional histological Hematoxylin-Eosin staining. Ad = digestive diverticulum in  
686 absorptive condition, ADd = digestive diverticulum in advanced digestive condition, al =  
687 adipocyte-like digestive cell, ar = acinar region, Bd = digestive diverticulum undergoing  
688 breakdown, bl = basal lamina, cs = positive anti-DA chromogenic signal, ct = connective  
689 tissue, dc = digestive cells, Dd = digestive diverticulum in digestive condition, dd = digestive  
690 duct, hc = hemocytes, Hd = digestive diverticulum in holding condition, ib = inclusion bodies,  
691 rb = residual bodies, Rd = diverticulum showing regeneration, sc = secretory cells, tr =  
692 tubular region. Scale bar:  $40\times = 50 \mu\text{m}$ ,  $63\times = 30 \mu\text{m}$ ,  $100\times = 10 \mu\text{m}$ .



693

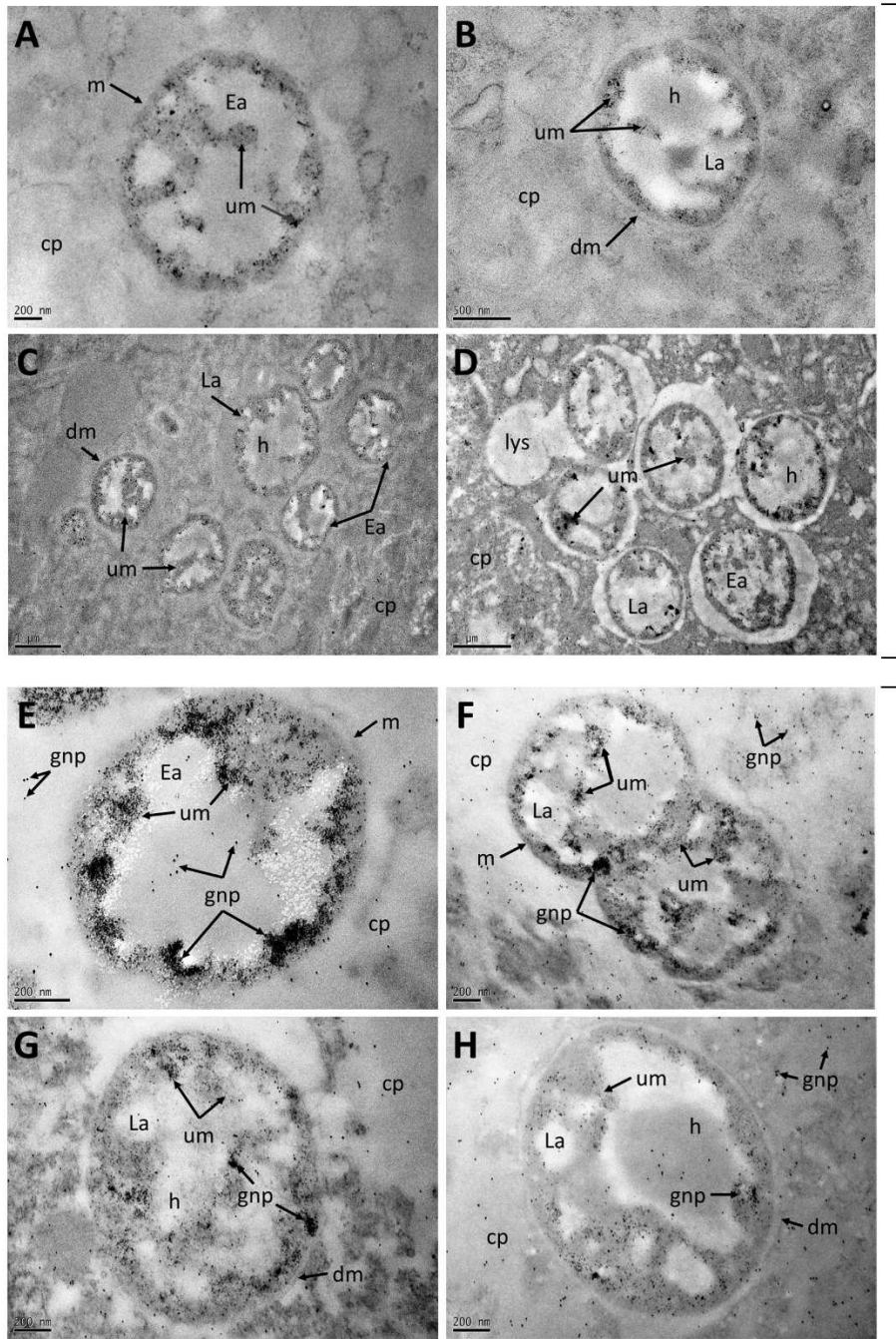
694 **Figure 3.** Microphotographs of digestive glands of scallops *P. maximus* naturally low  
 695 contaminated with  $\sim 2 \text{ mg DA kg}^{-1}$  collected at the Bay of Brest (n = 7) on the northwest coast  
 696 of France in December 2020. (A-B) specific anti-DA immunohistochemical (IHC) staining  
 697 incubated with the primary and secondary antibodies (1: 1,000 and 1: 10,000, respectively);  
 698 (C-D) negative controls of the IHC staining incubated with the secondary antibody but  
 699 without the primary anti-DA antibody (1: 10,000 and 1: 0, respectively); (E-F) conventional  
 700 histological Hematoxylin-Eosin staining. Ad = digestive diverticulum in absorptive condition,  
 701 al = adipocyte-like digestive cell, ar = ascinar region, Bd = digestive diverticulum  
 702 undergoing breakdown, bl = basal lamina, cs = positive anti-DA chromogenic signal, ct =  
 703 connective tissue, dc = digestive cells, Dd = digestive diverticulum in digestive condition, hc  
 704 = hemocytes, Hd = digestive diverticulum in holding condition, rb = residual bodies, Rd =  
 705 diverticulum showing regeneration, sc = secretory cells, tb = tubular region.





706

707 **Figure 4.** Microphotographs of the rest of the tissues of scallops *P. maximus* naturally  
 708 contaminated between  $\sim 2$  and  $750 \text{ mg DA kg}^{-1}$  collected at three sites (Concarneau [ $n = 6$ ],  
 709 Bay of Brest [ $n = 7$ ], and Camaret-sur-mer [ $n = 7$ ]) of the northwest coast of France between  
 710 2019 and 2021. (A-D) Specific anti-DA immunohistochemical (IHC) staining incubated with  
 711 the primary and secondary antibodies (1: 1,000 and 1: 10,000, respectively); (E-H) negative  
 712 controls of the IHC staining incubated with the secondary antibody but without the primary  
 713 anti-DA antibody (1: 10,000 and 1: 0, respectively); (I-L) multichromic histochemical  
 714 staining for the demonstration of neutral carbohydrates (violet-magenta dyes), acid  
 715 glycoconjugates (blue hues), and proteins (yellowish tones); (M-P) conventional histological  
 716 Hematoxylin-Eosin staining. bl = basal lamina, cs = positive anti-DA chromogenic signal, ct  
 717 = connective tissue, gd = gonadic duct, hc = hemocytes, lu = lumen, m = mucus, mc =  
 718 mucocyte, o = oocyte, of = ovarian follicle, pce = pseudostratified columnar epithelium, sg =  
 719 spermatogonia, spd = spermatids, spz = spermatozoa, ta = testicular acinus. Scale bar:  $40\times =$   
 720  $50 \mu\text{m}$ .



721

722 **Figure 5.** Electronmicrographs of ultrathin sections (70-80 nm) across the digestive glands of  
 723 scallops *P. maximus* naturally contaminated ( $\sim 75 \text{ mg DA kg}^{-1}$ ) during outbreaks of the toxic  
 724 *Pseudo-nitzschia* spp. and collected in Camaret-sur-mer ( $n = 7$ ) on the northwest coast of  
 725 France in 2021. Detection of autophagic structures with positive DA immune-signal within  
 726 digestive cells was possible by means of transmission electron microscopy (TEM). (1A-D)  
 727 Negative controls of the immunogold labeling incubated with the secondary antibody but  
 728 without the primary anti-DA antibody (1: 200 and 1: 0, respectively); (2E-H) Specific anti-  
 729 DA immunogold labeling incubated with the primary anti-DA antibody and the secondary  
 730 antibodies conjugated with 6-nm gold nanoparticles (1: 200 and 1: 500, respectively). cp =  
 731 cytoplasm, dm = double-membrane-bound, Ea = early autophagosomes, gnp = gold  
 732 nanoparticles, h = halo, La = late autophagosomes, lys = lysosomes, m = single-membrane-  
 733 bound, um = undigested material.